Mon. Not. R. Astron. Soc. **391,** 1605–1618 (2008) doi:10.1111/j.1365-2966.2008.14018.x

Properties of the ultraviolet flux of Type Ia supernovae: an analysis with synthetic spectra of SN 2001ep and SN 2001eh

D. N. Sauer,[1,5⋆] P. A. Mazzali,[1,2,5] S. Blondin,[3,4,5] M. Stehle,[1] S. Benetti,[2] P. Challis,[4] A. V. Filippenko,[6] R. P. Kirshner,[4,5] W. Li[6] and T. Matheson[7]

[1]*Max-Planck-Institut für Astrophysik, Karl-Schwarzschild-Str. 1, 85748 Garching, Germany*
[2]*Istituto Nazionale di Astrofisica-OAPd, vicolo dell'Osservatorio 5, 35122 Padova, Italy*
[3]*European Southern Observatory, Karl-Schwarzschild-Str. 2, 85748 Garching, Germany*
[4]*Harvard–Smithsonian Center for Astrophysics, 60 Garden Street, Cambridge, MA 02138, USA*
[5]*Kavli Institute for Theoretical Physics, University of California, Santa Barbara, CA 93106-4030, USA*
[6]*Department of Astronomy, University of California, Berkeley, CA 94720-3411, USA*
[7]*National Optical Astronomy Observatory, 950 N. Cherry Avenue, Tucson, AZ 85719-4933, USA*

Accepted 2008 September 26. Received 2008 September 26; in original form 2008 March 6

ABSTRACT

The spectral properties of Type Ia supernovae in the ultraviolet (UV) are investigated using the early-time spectra of SN 2001ep and SN 2001eh obtained using the *Hubble Space Telescope*. A series of spectral models is computed with a Monte Carlo spectral synthesis code, and the dependence of the UV flux on the elemental abundances and the density gradient in the outer layers of the ejecta is tested. A large fraction of the UV flux is formed by reverse-fluorescence scattering of photons from red to blue wavelengths. This process, combined with ionization shifts due to enhanced line blocking, can lead to a stronger UV flux as the iron-group abundance in the outer layers is increased, contrary to previous claims.

Key words: radiative transfer – supernovae: general – supernovae: individual: SN2001ep – supernovae: individual: SN 2001eh – cosmology: observations.

1 INTRODUCTION

Type Ia supernovae (SNe Ia) are among the most important tools to study the expansion history of the Universe and to set constraints on the properties of dark energy (Riess et al. 1998; Perlmutter et al. 1999; Tonry et al. 2003; Riess et al. 2004; Astier et al. 2006; Riess et al. 2007; Wood-Vasey et al. 2007; see Leibundgut 2001; Filippenko 2004, 2005 for reviews). With the empirical calibration of their peak luminosity (Phillips 1993; Phillips et al. 1999; Jha, Riess & Kirshner 2007), it is feasible to probe the properties of the Universe out to a redshift of $z \approx 1$ and higher (Goldhaber et al. 2001; Tonry et al. 2003; Riess et al. 2004, 2007). Understanding the formation of the ultraviolet (UV) spectrum of SNe Ia is important for two reasons: the optical spectrum is strongly affected by line blocking in the UV and optical observations of high-redshift supernovae primarily cover the rest-frame *UV* bands. Comparisons between local and distant SNe Ia have recently identified the UV as an important region to search for possible effects of evolution (Foley et al. 2008; Bronder et al. 2008; Ellis et al. 2008).

Efforts have been made to increase the sample of local SNe Ia observed in the UV by space-borne telescopes. The amount of data available for SNe Ia in the UV is very small and mostly limited to single epochs – usually around (or well after) maximum light (Panagia 2003; Foley, Filippenko & Jha 2008). Prominent examples include the *Hubble Space Telescope* (*HST*) spectra of SN 1992A (5 and 45 d after *B*-band maximum, Kirshner et al. 1993) and the very early *International Ultraviolet Explorer* (*IUE*) spectrum of SN 1990N (14 d before *B*-band maximum, Leibundgut et al. 1991). Recently, the ultraviolet/optical telescope (UVOT) onboard the *Swift* satellite (Gehrels et al. 2004) has also provided valuable UV data on SNe Ia (Immler et al. 2006).

To interpret such data correctly, it is necessary to understand the formation of the UV flux in SNe Ia and its sensitivity to physical parameters of the explosion and ambient medium. Several groups have studied the properties of the UV flux using radiative transfer models of differing complexity (Pauldrach et al. 1996; Fisher et al. 1997; Höflich, Wheeler & Thielemann 1998; Mazzali 2000; Lentz et al. 2001).

In this paper, we use radiative transfer models to study the properties of SN 2001eh and SN 2001ep, which were observed as part of the Supernova INtensive Study (SINS; GO−9114; PI R. P. Kirshner) with *HST*. Based on the spectral models, we investigate how a change of physical parameters may affect the observed UV flux of a SN Ia. In particular, when using SNe Ia as standard candles to measure cosmological parameters, it is important to know if parameters that are likely to change over a large range of redshifts can introduce systematic errors in the distance measurement. Among the parameters that may be affected by the environment of SN Ia progenitors is the abundance of heavy elements in the outer

⋆E-mail: dsauer@mpa-garching.mpg.de

shells of the ejecta. These layers are of particular importance for the formation of the UV spectrum during the photospheric phase. The two supernovae chosen for this study are at the opposite ends of the luminosity distribution of normal SNe Ia.

From spectral analysis of SNe Ia, we know that the composition is dominated by a mixture of intermediate-mass elements, such as Si, S and Mg, and iron-group elements (Ni, Co and Fe). At early epochs, until a few weeks after maximum brightness, the spectrum of a SN Ia consists of a number of broad absorption troughs that generally originate from blends of various lines. (For a review of the observed properties of SNe Ia, see Filippenko 1997 and Leibundgut 2000.) The emission of SNe Ia is entirely powered by the radioactive decay of ^{56}Ni created in the explosion. The γ-ray photons from radioactive decay undergo Compton scattering, creating fast electrons which deposit their energy via collisions in the expanding ejecta (Truran, Arnett & Cameron 1967; Colgate & McKee 1969). The non-thermal continuum seen at early epochs around maximum light is formed by the overlap of thousands of weaker lines. The spectrum peaks at a wavelength between 4000 and 5000 Å and drops steeply in the UV, bluewards of the Ca H&K lines, which typically have an absorption minimum at about 3750 Å near maximum light (Blondin et al. 2006).

The UV wavelength bands of SNe Ia comprise only a small fraction of the total emitted light, and are generally characterized by the absence of strong features. Singly and doubly ionized species of heavy elements such as Ti, Cr, Fe, Co and Ni have a large number of line transitions in the *UV* bands that effectively block most of the emission in these bands (Karp et al. 1977; Höflich, Müller & Khokhlov 1993; Pauldrach et al. 1996). Lucy (1999b) and Mazzali (2000) find that essentially all UV photons created at deeper layers in the ejecta are immediately absorbed and down-scattered to lower energies (longer wavelengths) where the line opacity is smaller. The crucial mechanism for the emission of photons in the UV is found to be a reverse-fluorescence process where absorption of red photons is followed by emission in the blue and *UV* bands (Lucy 1999b; Mazzali 2000). These processes have a significantly lower probability of occurrence but in the outer region of the ejecta the emission of bluer photons via reverse fluorescence can be significant because there are many more red photons available than blue ones such that the lines in the blue are not saturated. Blue photons can escape from a line rather than getting re-absorbed locally. The UV spectrum is predominantly shaped by this fluorescence spectrum originating from a confined layer of high-velocity material, which is small compared to the dimensions of the expanding ejecta (Mazzali 2000). The shape of the emission spectrum is determined by the atomic properties of the ions in the emission layer. This makes the UV an interesting wavelength band in which to study possible progenitor scenarios because the progenitor star may leave a characteristic imprint on the composition of the outermost layers of the expanding shell.

Lentz et al. (2001) investigated the dependence of the UV flux of SNe Ia on the composition of the outermost layers of the ejecta, adopting different fractions of solar metallicity for the material above $v \approx 14\,000\,\mathrm{km\,s^{-1}}$. They found that overall the UV flux decreases with increasing metallicity. They also pointed out, however, that the larger number of strong absorption lines with higher metallicity can cause a back reaction of the blocked radiation field on the temperature and ionization structure (line blanketing), which is difficult to disentangle from the line-blocking effect. Therefore, the UV flux may vary non-linearly with a change of composition.

In this paper, we investigate the sensitivity of the UV spectrum to modifications of the composition in the outer layers. We also consider variations in the density structure of the underlying explosion model.

The paper is organized as follows. In Section 2, we present observations of SN 2001ep and SN 2001eh covering the UV wavelength range as an example of SNe Ia with different UV properties. Section 3 outlines the radiative transfer code used for this work and an analysis of the observed spectra with the help of synthetic spectra. The radiative transfer models for both supernovae are used as a basis for a series of models to study the properties of the UV flux with respect to the changes in composition and density structure. The results of this series and the physical processes responsible for the formation of the UV flux are discussed in Section 4. Section 5 gives the conclusions of our study.

2 OBSERVATIONS

We present observations and synthetic spectra of SN 2001eh and SN 2001ep as examples of SN Ia that exhibit significantly different spectral properties, especially in the UV. A more detailed discussion of the complete data available for the two supernovae (*UBVRI* light curves, optical spectra and one additional UV spectrum for each SN) will be presented in a forthcoming paper (Blondin et al., in preparation). Here, we present the data relevant to the study of the UV spectra discussed in this paper. The observations are summarized in Table 1.

SN 2001eh was discovered on 2001 September 9 (UT dates are used throughout this paper) by M. Armstrong (Hurst & Armstrong 2001) and independently by M. Ganeshalingam and W. D. Li (Ganeshalingam et al. 2001) with the Katzman Automatic Imaging Telescope (KAIT; Filippenko et al. 2001) as part of the Lick

Table 1. UV and optical spectra of SN 2001eh and SN 2001ep.

IAU name	UT date	Telescope + Instrument	Slit (arcsec)	Grating	Range (Å)	Exptime (s)
2001eh	2001 September 25.67	*HST* + STIS	52 × 0.2	G140L	1140–1730	1340
2001eh	2001 September 25.76	*HST* + STIS	52 × 0.2	G230L	1570–3180	2 × 2700
2001eh	2001 September 25.66	*HST* + STIS	52 × 0.2	G430L	2900–5700	500
2001eh	2001 September 26.35	FLWO 1.5 m + FAST	3	300	3720–7540	1200
2001eh	2001 September 26.37	FLWO 1.5 m + FAST	3	300	5200–9040	1200
2001ep	2001 October 27.99	*HST* + STIS	52 × 0.2	G140L	1140–1730	1630, 2690
2001ep	2001 October 28.09	*HST* + STIS	52 × 0.2	G230L	1570–3180	2690
2001ep	2001 October 27.95	*HST* + STIS	52 × 0.2	G430L	2900–5700	200
2001ep	2001 October 25.42	FLWO 1.5 m + FAST	3	300	3720–7540	1200
2001ep	2001 October 25.44	FLWO 1.5 m + FAST	3	300	5200–9040	1200

Observatory and Tenagra Observatory Supernova Search (LOTOSS). It occurred in UGC 1162, which have a NASA/IPAC Extragalactic Data base (NED)[1] recession velocity of $cz = 11\,131\,\mathrm{km\,s^{-1}}$ (from The Updated Zwicky Catalog;[2] Falco et al. 1999). A CCD spectrum obtained on September 11 with the Shane 3-m reflector at Lick Observatory revealed that SN 2001eh was a SN Ia about a week before maximum brightness (Ganeshalingam et al. 2001).

SN 2001ep was discovered on 2001 October 3 by Hutchings & Li (2001) as part of LOTOSS. It occurred in NGC 1699, which has a NED recession velocity of $cz = 3901\,\mathrm{km\,s^{-1}}$ (de Vaucouleurs et al. 1991). A CCD spectrum obtained on 10 October with the Fred L. Whipple Observatory (FLWO) 1.5-m Tillinghast telescope and FAST spectrograph (Fabricant et al. 1998) showed that it was a SN Ia near maximum brightness (Matheson et al. 2001).

SN 2001eh and SN 2001ep were observed with *HST* (Cycle 10) as targets of opportunity. The data were obtained with the Space Telescope Imaging Spectrograph (STIS) using a 52×0.2 arcsec^2 slit. For both supernovae, we used the G430L grating to obtain 'optical' spectra (2900–5700 Å), the G230L grating to obtain near-UV spectra (1600–3100 Å) and the G140L grating to obtain far-UV spectra (1150–1700 Å). No clear signal was detected for any observation taken with the latter setup. The reductions followed the standard STIS reduction pipeline. Spectra were extracted from the processed images using the IRAF[3] SPECRED long-slit reduction packet.

The optical spectra presented in this paper were obtained with the FLWO 1.5-m FAST spectrograph using a slit of width 3 arcsec. For both supernovae, we used a 300 line mm^{-1} grating with two tilts: one covering ∼3700–7500 Å, the other ∼5200–9000 Å. The spectra were reduced and calibrated employing standard techniques in IRAF and our own IDL routines for flux calibration.

The KAIT *B*-band light curves for SN 2001eh and SN 2001ep are shown in Fig. 1. Both are sufficiently well sampled to enable a direct measurement of the decline-rate parameter $\Delta m_{15}(B)$. For SN 2001eh, we find $\Delta m_{15}(B) = 0.71 \pm 0.05$, while for SN 2001ep we find $\Delta m_{15}(B) = 1.41 \pm 0.04$. Thus, SN 2001eh is a 'slow decliner', while SN 2001ep is at the fast end of typical 'intermediate-decliner' SNe Ia.

The differences in light-curve shape between the two supernovae are reflected in their spectra. Using the Supernova Identification (SNID) cross-correlation code of Blondin & Tonry (2007), we find that the best match for SN 2001eh is the overluminous SN 1999aa [$\Delta m_{15}(B) = 0.75 \pm 0.02$; Krisciunas et al. 2000] and the best-match template spectrum for SN 2001ep is the 'transitional' SN 2004eo [$\Delta m_{15}(B) = 1.45 \pm 0.04$; Pastorello et al. 2007].

We fitted the complete *UBVRI* photometric data with the MLCS2k2 light-curve fitter of Jha et al. (2007). The time of *B*-band maximum is found to be 2001 September 17.53 (JD = 245 2170.03 ± 0.71) for SN 2001eh and October 17.72 (JD = 245 2200.22 ± 0.45) for SN 2001ep. The derived line-of-sight extinction in the host galaxy is $A_V = 0.08 \pm 0.06$ and 0.43 ± 0.12 mag, respectively. The Milky Way foreground reddening is small for both supernovae [$E(B-V) = 0.06$ mag for SN 2001eh and $E(B-V) = 0.05$ mag for SN 2001ep; Schlegel, Finkbeiner & Davis 1998].

[1] The NED is available at http://nedwww.ipac.caltech.edu.

[2] http://tdc-www.harvard.edu/uzc/

[3] IRAF is distributed by the National Optical Astronomy Observatories, operated by the Association of Universities for Research in Astronomy, Inc., under contract to the National Science Foundation of the United States.

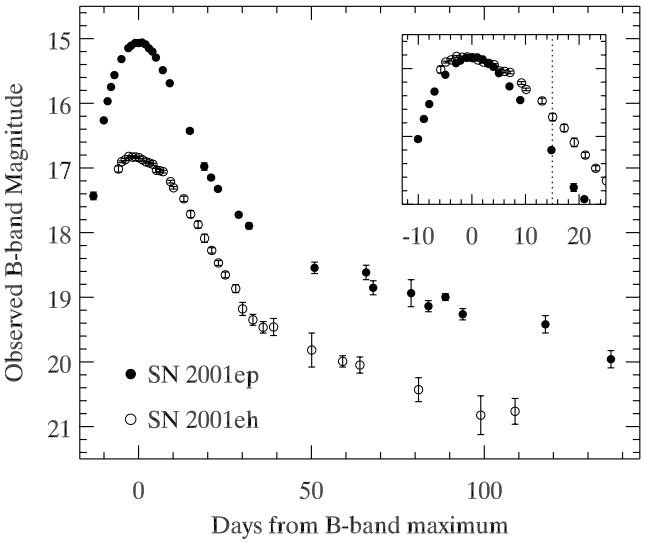

Figure 1. KAIT *B*-band light curves of SN 2001eh and SN 2001ep. The inset shows both light curves out to ∼20 d past *B*-band maximum, normalized in magnitude at the peak. The dotted line at +15 d highlights the difference in $\Delta m_{15}(B)$ between the two supernovae (see the text for details).

The UV and optical spectra of each SN were combined into a single spectrum. The far-UV data taken with the G140L grating were not included in either of the combined spectra given the lack of signal. The mean UT date for the SN 2001eh spectrum is 2001 September 25.93, corresponding to ∼9 d past *B*-band maximum. The mean UT date for the SN 2001ep spectrum is 2001 October 26.88, also corresponding to ∼9 d past *B*-band maximum. Assuming a *B*-band rise time of ∼19.5 d (Conley et al. 2006; Riess et al. 1999), both spectra correspond to 28–29 d past explosion. In what follows, we assume that both spectra are at $t = 29$ d past explosion.

3 SPECTRAL MODELS

3.1 The radiative transfer model

To model synthetic spectra of SNe Ia at early epochs, we use a Monte Carlo spectral synthesis code with an approximate description of non-local thermodynamic equilibrium (non-LTE) (i.e. not assuming LTE). Here, we outline the most important aspects of our method as they are relevant for the discussion in this work. More detailed descriptions can be found in Abbott & Lucy (1985), Mazzali & Lucy (1993) and Lucy (1999b), as well as in Mazzali (2000). This last reference also gives the sources of atomic data used by the code.

For the underlying explosion model, we take the density structure from the one-dimensional deflagration model W7 (Nomoto, Thielemann & Yokoi 1984). The composition is adjusted to match the observed spectrum. For this study, we use the version of the code that allows a radial variation of the composition within the ejecta described by Stehle et al. (2005).

The code is based on the Schuster–Schwarzschild approximation – that is, we assume that the radiative energy is entirely emitted at the inner boundary of the computational grid with the spectral shape of a blackbody. The spectra are calculated assuming stationarity and ignoring any time dependences. This is a good approximation at least for one-dimensional models of SN Ia later than a few days after explosion (Kasen, Thomas & Nugent 2006). We do not consider the deposition of energy by γ-ray photons from the ^{56}Ni and ^{56}Co

decays within the atmosphere, nor do we try to derive the total luminosity directly from the ^{56}Ni mass. Therefore, luminosity is a free parameter. To constrain the model, the location of the inner boundary ('photosphere')[4] has to be specified in terms of a velocity $v_{\rm ib}$ and the elapsed time t since the explosion, assuming homologous expansion [$r(t) = v$] of the ejecta. In addition to those physical input parameters, observational parameters such as distance and reddening have to be specified to allow direct comparison of the synthetic and the observed spectrum.

The code uses an approximate description of non-LTE to derive the atomic level populations and the ionization equilibrium. Collisional and continuum processes are not considered, apart from electron scattering. Since the opacity in SN Ia ejecta is largely dominated by the opacity of Doppler-shifted and broadened spectral lines, the true continuum plays only a minor role. Given the low densities in the ejecta, collisional processes are also not expected to have a major impact on the state of the gas. It is not possible to derive a consistent gas temperature in this approximation. Thus, following Mazzali & Lucy (1993), the local gas temperature is approximated to be 90 per cent of the radiation temperature $T_{\rm R}$ of the radiation field, which is determined from the mean energy $\bar{x}$ of a photon in a Planckian radiation field:

$$\bar{x} = \frac{h\bar{\nu}}{k_{\rm B}T} = \frac{h}{k_{\rm B}T}\frac{\int_0^\infty \nu B_\nu \,{\rm d}\nu}{\int_0^\infty B_\nu \,{\rm d}\nu} = \frac{360}{\pi^4}\zeta(5) \approx 3.832 \quad (1)$$

(see also Lucy 1999a). The temperature of the blackbody at the inner boundary is determined in an iteration cycle, using the constraint that the desired luminosity L is obtained at the outer boundary. Iteration is necessary because the amount of radiation that is scattered back into the core is not known a priori.

A crucial quantity for the derivation of the ionization and excitation equilibrium is the 'equivalent dilution factor' W introduced by Mazzali & Lucy (1993). This factor, which is derived from the nebular approximation for the radiation field in an optically thin medium, is used to modify the LTE Saha–Boltzmann excitation formula. While in a gaseous nebula W describes a purely geometrical dilution of the radiation field, the procedure developed for supernova ejecta derives W directly from the assumed relationship between the Planck function at the radiation temperature $T_{\rm R}$ and the radiation field J:

$$J = W B(T) = W\frac{\sigma}{\pi}T_{\rm R}^4, \quad (2)$$

where σ denotes the Stefan–Boltzmann constant. This approximation has been shown to produce a reasonably good representation of non-LTE ionization and excitation in supernova ejecta (Mazzali & Lucy 1993).

Line processes are treated using the line-branching formalism introduced by Lucy (1999b) and Mazzali (2000). While earlier work with this code assumed pure resonant scattering of photons in spectral-line transitions, this improvement allows photons to be re-emitted in a different transition than the one by which they were absorbed. Mazzali (2000) showed that the inclusion of branching processes is necessary to reproduce the flux in the UV.

[4] We generally avoid the term 'photosphere' for this inner boundary. In contrast to stars, where this term refers to the radius at which the atmosphere becomes optically thick with respect to a wavelength-independent *mean* optical depth, this concept cannot be used in hydrogen-deficient supernovae, where the optical-depth scale is strongly wavelength-dependent owing to the shallow density gradient and the absence of strong continuum opacities (see e.g. Sauer, Hoffmann & Pauldrach 2006).

Following the description of Lucy (1999b), the emergent spectrum is derived by a formal solution of the transfer equation using line and continuum source functions that are extracted from the Monte Carlo simulation. The advantage of this method over using emerging Monte Carlo packets directly is a significantly reduced number of Monte Carlo packets to obtain a converged spectrum with low Monte Carlo noise. Because the UV flux of a SN Ia is intrinsically very low, one must nevertheless ensure that the number of packets used in the Monte Carlo experiment is sufficient to provide a converged solution for the source functions. We performed convergence tests in the UV and determined that the relative scatter of the spectrum caused by Monte Carlo noise in the wavelength range between 1500 and 3000 Å is generally well below 10 per cent for 500 000 photon packets. With this number, the scatter in the optical spectrum is less than 0.4 per cent.

3.2 Synthetic spectra for SN 2001ep and SN 2001eh

The models and the observed spectrum of SN 2001eh are shown in Fig. 2(a); those of SN 2001ep are shown in Fig. 2(b). The inserts in the figures show the UV part of the spectra on a logarithmic scale. The direct comparison of both observed spectra clearly shows that these supernovae exhibit fairly different spectral appearances. In SN 2001eh, the UV flux blue of Ca II H&K at ∼3750 Å is stronger with relation to the optical spectrum. The characteristic line features are fairly narrow and found at lower velocities than in the spectrum of SN 2001ep.

Modelling the spectra requires knowledge of the distance and reddening of the supernovae. For the distance, we use the data available for the respective host galaxies listed in NED. The redshift of the host galaxy of SN 2001eh (UGC 1162, $z = 0.037$) corresponds to a distance modulus of $m - M = 35.9$ mag assuming $H_0 = 73\,{\rm km\,s^{-1}\,Mpc^{-1}}$ (Riess et al. 2005). NGC 1699, the host galaxy of SN 2001ep, has a redshift of $z = 0.013$, resulting in a distance modulus of $m - M = 33.6$ mag. For the model of SN 2001eh, we assume a total reddening of $E(B - V) = 0.07$ mag, while for SN 2001ep we use $E(B - V) = 0.15$ mag. The value for the reddening of SN 2001ep is at the lower end of the uncertainty range estimated from observational indicators (see Section 2); higher values for $E(B - V)$, however, require a higher luminosity and lead to a shift in the ionization towards doubly ionized species of Fe and Co that are not seen in the observed spectrum.

For both supernovae, the epoch was taken to be 29 d after explosion (see Section 2). The synthetic spectrum of SN 2001eh was modelled with a luminosity of $L = 1.15 \times 10^{43}\,{\rm erg\,s^{-1}}$. For the spectrum of SN 2001ep, we need a lower luminosity of $L = 7.98 \times 10^{42}\,{\rm erg\,s^{-1}}$. For both models, we adopted the density structure from the W7 explosion model (Nomoto et al. 1984); the composition was adjusted to fit the observed spectrum. To model SN 2001eh, we set the velocity of the inner boundary to $v_{\rm ib} = 5200\,{\rm km\,s^{-1}}$. For SN 2001ep, we used $v_{\rm ib} = 5000\,{\rm km\,s^{-1}}$. Above the inner boundary, the ejecta were divided into several radial zones where the composition was adjusted independently. The composition of the outer zones was determined using the spectra of earlier epochs available for both supernovae. The outcome of theoretical explosion models such as W7 and the results of tomography studies of SN Ia with similar properties (SN 2002bo Stehle et al. 2005 for SN 2001eh and SN 2004eo Mazzali et al. 2008 for SN 2001ep) served as a rough guideline. The inner region ($v \lesssim 8000\,{\rm km\,s^{-1}}$) of the ejecta of SN 2001eh contains mostly (>80 per cent) elements generated by burning to nuclear statistical equilibrium (NSE; Fe-group material, mostly ^{56}Ni). This is followed by a layer containing ∼60 per cent intermediate-mass

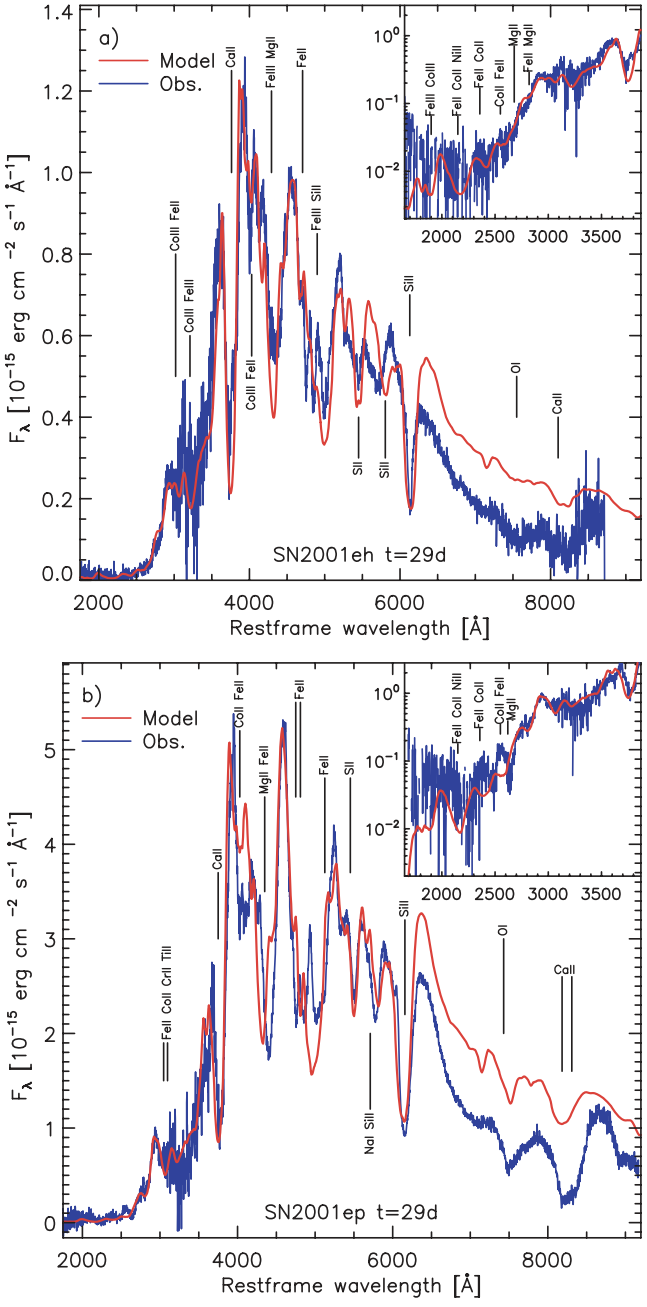

Figure 2. Synthetic and observed spectra of (a) SN 2001eh and (b) SN 2001ep, both at $t = 29$ d after explosion. The inserts show the UV part of the respective spectra with a logarithmic scale. The labels indicate the ions that dominate the formation of the various absorption features. The blue and UV parts of the spectrum are formed by a blend of a large number of lines, precluding a complete identification of the contributors.

elements (IME) (Si, S, Mg, Ca) and ∼20 per cent of NSE material out to 12 000 km s^{-1}. The layers above 12 000 km s^{-1} are dominated by unburned O and C (58–98 per cent) with small amounts of IME (between 2 and 20 per cent) and NSE material (0.5–4.5 per cent), decreasing outwards. In the less luminous SN 2001ep, the IME-rich region extends to lower velocities (∼6000 km s^{-1}) and the O-rich layer reaches down to ∼9000 km s^{-1}. The mass fraction of NSE material appears to drop rapidly ($\lesssim$25 per cent) above ∼7000 km s^{-1}. In the outermost layers above ∼10 000 km s^{-1}, the mass fraction of IME material drops from ∼40 to 1 per cent outwards, NSE material from 3 to 0.2 per cent; the NSE abundance in the outer layers is somewhat lower than in SN 2001eh which is in line with the findings of Mazzali et al. (2007). The presence of small amounts of NSE material in the outermost layers is, however, necessary to fit the UV part of the spectrum in both supernovae. The original W7 density structure only extends to a velocity of 24 000 km s^{-1}. To ensure that the choice of the maximum velocity of the computational grid does not affect the outcome of the model, the density structure is extrapolated to higher velocities using the power-law index of the outer zones of the input-density structure. In the model series discussed later in this paper, the maximum velocities are set to large values (∼70 000 km s^{-1}) to avoid artefacts generated by this boundary.

The models fit the spectra fairly well in the UV and optical parts of the spectrum. The offset in the wavebands redwards of the Si II feature at ∼6100 Å is caused by the breakdown of our assumption of a thermal lower boundary. The opacity at these wavelengths is dominated by electron scattering, which does not modify the spectral properties of the radiation field. The radiation at these wavelengths originates from layers below our adopted inner boundary and is shaped by a large number of individually weak lines (Kasen 2006). With our assumption of stationarity and the chosen set of atomic data, the shape of the pseudo-continuum cannot be correctly described by the model even if extended to deeper layers (Sauer, Hoffmann & Pauldrach 2006). Additionally, a description of the ejecta below the lower boundary implies that we rely on specific explosion models, which introduce additional uncertainties. The absorption features blue of ∼2700 Å in the spectrum of SN 2001ep (insert of Fig. 2b) appear to be too blue in the synthetic fit. This mismatch probably indicates that the outer part of the density structure used to compute the model is not appropriate. This is not surprising given that the W7 model generated more ^{56}Ni than what is expected for SN 2001ep and may therefore also have a larger kinetic energy than required to describe this SN. Another indication of an incorrect density structure is that the model fails to reproduce the separated Fe II features around 5000 Å which produce the apparent emission feature at ∼4950 Å.

The major absorption features are labelled in Fig. 2. However, especially towards the blue and UV, where the features are blends of many different lines, ions other than those indicated in the plot also contribute to the shape of the absorption. SN 2001eh is bluer than SN 2001ep and has a different spectral appearance at the same epoch. The spectrum of SN 2001eh contains a significant contribution from doubly ionized species such as Fe III and Co III, while the spectrum of SN 2001ep is dominated by lines of singly ionized species. The characteristic Fe II features (e.g. between 4500 and 5000 Å) are significantly weaker in SN 2001eh than in SN 2001ep. The comparison of the dominant ionization stages indicates that the gas temperatures in the ejecta of SN 2001eh are higher than in SN 2001ep. In the models of SN 2001ep, the temperatures at similar velocities are generally 500–1000 K lower than in the SN 2001eh model.

More differences are visible in the region bluewards of Ca II H&K. Relative to the optical emission peaks, SN 2001eh has substantially more flux in this region than SN 2001ep. Further to the UV the Mg II 2800 Å absorption, which dominates the shape of the spectrum in the region around 2600 Å, is stronger in SN 2001ep.

The differences seen in the UV result from different compositions or densities of the outermost layers of the ejecta. In particular, Fe-group ions from Ti to Ni have a large number of spectral lines in the UV that lead to large optical depths out to the highest velocities where this part of the spectrum is shaped.

4 THE UV FLUX IN SN IA – A MODEL SERIES

We investigate the impact of ejecta properties on the observed flux in the UV using a series of parametrized models where we modified first the composition and then the density gradient in the outer layers. Composition is expected to be the primary quantity responsible for changes in the UV spectrum (see e.g. Lentz et al. 2001). In addition, the imprint of a progenitor is likely to manifest itself as a variation of the composition in the outer layers. A modified density structure can also be responsible for changes in the appearance of the UV spectrum. Different explosion models predict variations in density, in particular at the higher velocities. Specifically, models with a deflagration-to-detonation transition (DDT) occurring at some stage during the explosion accelerate the matter to higher velocities resulting in higher densities and more burned material in the outer layers of the ejecta (Khokhlov 1991; Höflich, Khokhlov & Wheeler 1995; Iwamoto et al. 1999; Röpke & Niemeyer 2007; Röpke 2007).

4.1 Variation of the composition

4.1.1 Setup

We use the models discussed in the previous section to setup a parametrized model series in which the abundance of heavy elements is varied stepwise in the outermost zone. For the first test series, we keep the density structure of the model unchanged and balance the modification of heavy element abundances with a change of the oxygen abundance. In the outer layers of the models, O is the most abundant element and causes very few visible features in the early-time spectrum of SNe Ia. Therefore, even drastic changes in the oxygen abundance do not affect the spectral appearance; the models primarily reflect the effects of a variation in the abundance of heavy elements. (For the most extreme cases, a change of the electron density may become significant. A composition dominated by oxygen can provide more electrons per unit mass than IME or Fe-group elements. Most of this effect is, however, counterbalanced by the higher ionization potential of oxygen resulting in a larger fraction of neutral atoms than for heavier elements.)

Within each series all model parameters are kept constant and only the abundance of a specific element or group of elements is increased or decreased above a velocity $v_{\rm shell}$. For the models of SN 2001eh, we set $v_{\rm shell} = 15\,000\,{\rm km\,s^{-1}}$, while for the SN 2001ep based models we use $v_{\rm shell} = 14\,500\,{\rm km\,s^{-1}}$. The velocities are chosen to be roughly the range at which the radiation field in the optical wavelength bands is mostly decoupled from the ejecta matter (cf. Fig. 6). The compositions of the outer layers for the two base models are shown in Table 2. The models are calculated out to $v \sim 70\,000\,{\rm km\,s^{-1}}$ where the density is low enough to ensure that the outer cut-off velocity does not affect the model results. As for the original models, we use 500 000 Monte Carlo packets to keep the Monte Carlo induced noise in the UV spectrum sufficiently low.

We chose to vary the composition of (i) Fe alone (corresponding to stable Fe not produced via the ^{56}Ni-decay chain), (ii) ^{56}Ni (at the epoch of 29 d, this corresponds to 3.7 per cent Ni, 79.7 per cent Co and 16.6 per cent Fe[5]) and (iii) Ti and Cr together. The last two elements do not produce strong visible features in the spectrum, but affect the UV flux because they have a large number of relatively weak lines that densely cover the UV and therefore contribute significantly to the total opacity. For each base model, we increased and decreased the composition of the groups of elements in steps of 0.5 dex.

[5] Using half lives from Junde (1999).

Table 2. Outer layer composition (mass fractions) of the two base models. Fe listed here corresponds to Fe not generated in the ^{56}Ni-decay. The decay products of ^{56}Ni after $t = 29$ d are listed separately below.

	SN 2001eh	SN 2001ep
$v_{\rm shell}$	$15\,000\,{\rm km\,s^{-1}}$	$14\,500\,{\rm km\,s^{-1}}$
C	2.0×10^{-1}	8.0×10^{-2}
O	7.7×10^{-1}	8.3×10^{-1}
Mg	1.0×10^{-4}	1.0×10^{-4}
Si	5.0×10^{-3}	8.6×10^{-2}
S	2.0×10^{-2}	1.1×10^{-3}
Ca	1.5×10^{-3}	5.1×10^{-4}
Ti	3.0×10^{-4}	6.1×10^{-5}
Cr	3.0×10^{-4}	1.0×10^{-5}
Fe	5.0×10^{-4}	1.0×10^{-3}
^{56}Ni	5.0×10^{-3}	2.0×10^{-3}
^{56}Ni	1.8×10^{-4}	7.4×10^{-5}
^{56}Co	4.0×10^{-3}	1.6×10^{-3}
^{56}Fe	8.3×10^{-4}	3.3×10^{-4}

4.1.2 Results

The spectra of the series are shown in Fig. 3. The models in the left-hand column are based on SN 2001eh, the ones in the right-hand column on SN 2001ep. Each column shows the model for Fe variation alone in the upper plot, the ^{56}Ni series in the middle and the Ti/Cr series in the bottom plot. The insets show the UV part of the spectrum in logarithmic scaling for each set. The colour coding represents the different models – the shades of blue represent models in which the abundance of the element groups has been decreased, while the shades of red are models in which the abundances have been increased. For comparison, the original model is shown in black.

Overall, an increase in abundances has a stronger effect than a decrease. This is not surprising, because the abundance of heavy elements was already relatively low in the outer layers of the base models. The comparison of the three groups of models shows that the relative change of the optical part of the spectrum is small to moderate; the variation of Fe alone has the strongest effect on the optical part especially in the series of spectra based on SN 2001ep (Fig. 3, right-hand panels).

The variation of the blue and the UV part of the spectra differs among the different groups of models. In the SN 2001eh series, the absorption feature at 3050 Å becomes deeper with higher Fe abundance; in the SN 2001ep series, this feature does not change significantly. The region red of this feature, up to ∼3500 Å, shows significantly enhanced flux for higher Fe abundance in both the cases. In the SN 2001ep series, this higher flux level also affects the re-emission peak bluewards of the Ca II H&K feature, which remains mostly unchanged in the SN 2001eh models. The models where Fe is decreased are very close to the base model in both the series.

Further to the UV, bluewards of ∼2500 Å, the models based on SN 2001eh (Fig. 3, upper left-hand panel) show little change with the variation of the Fe abundance. In the corresponding SN

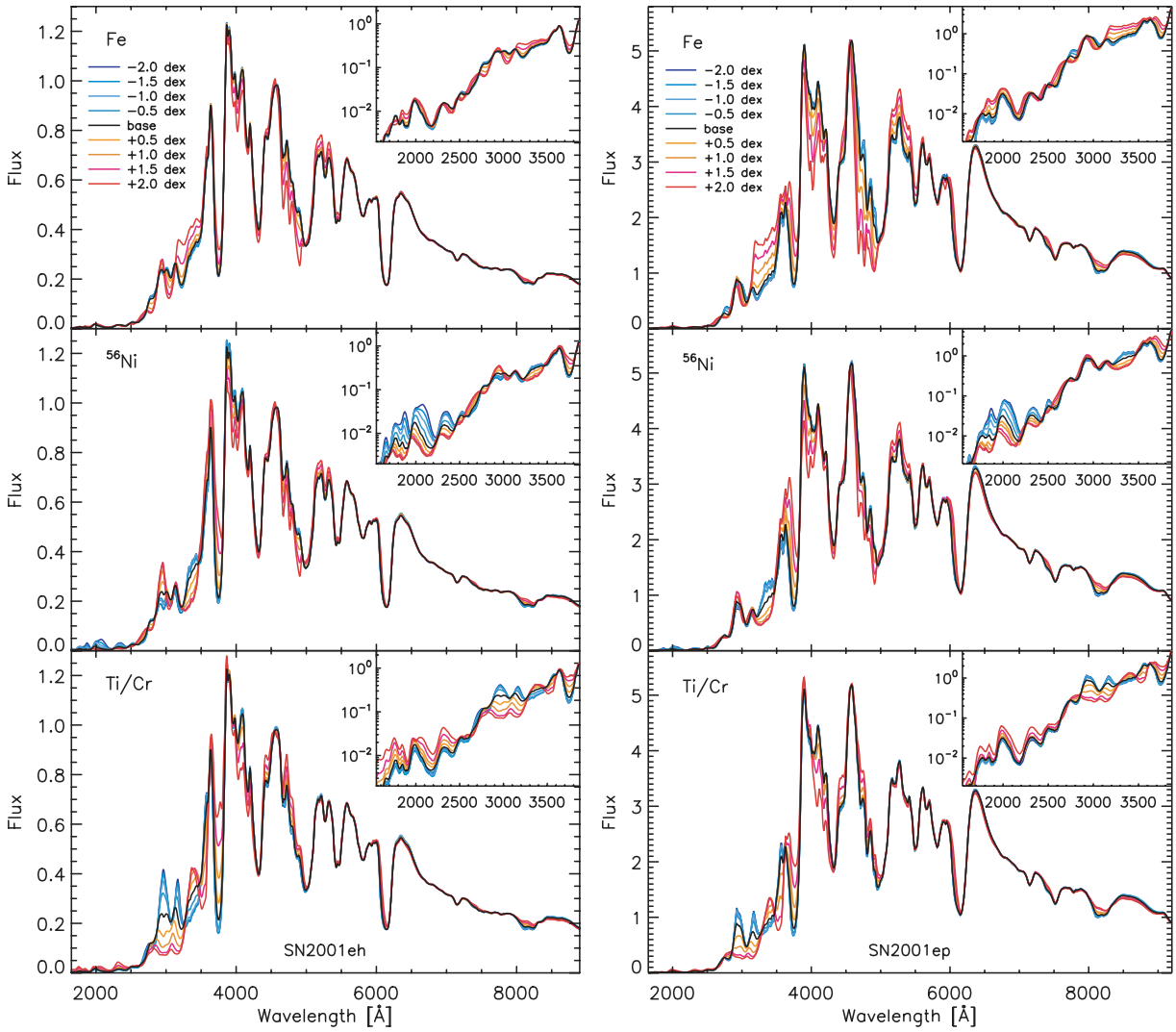

Figure 3. Model series for varying composition of the outer layers for the SN 2001eh based model series (left-hand column) and the SN 2001ep based model series (right-hand column). The upper panels show the series where Fe alone is varied, the middle panels show the series with a variation of ^{56}Ni (i.e. Ni, Co and Fe together) and the lower panels show the series for Ti and Cr. Colour coding indicates different models – blue lines represent models where the abundance of the respective element is decreased, red lines show models where the abundance is increased. The black line refers to the original model.

2001ep series (Fig. 3, upper right-hand panel), we observe the trend that models with higher Fe abundance have more flux in the UV, although the effect here is also small.

The variation of ^{56}Ni is visible in a similar region as in the Fe models, but with the opposite trend. Models with more ^{56}Ni have a deeper absorption at ∼3300 Å, which is mostly caused by stronger Co III lines. Consequently, the emission peak bluewards of the Ca II absorption become stronger in those models (this peak is largely induced by the P-Cygni re-emission of those Co lines). Again the variation in this peak is stronger in the SN 2001ep based models. In the UV part blue of about 2500 Å, the effect of decreasing the ^{56}Ni abundance leads to more flux while increasing the ^{56}Ni abundance leads to less flux.

The bottom panels of Fig. 3 show the models where the abundances of Ti and Cr have both been varied. The most prominent result of this variation is the change of the double-peaked re-emission feature centred at 3000 Å. For low Ti and Cr abundances in the outer layers, this double-peaked structure becomes more and more prominent, while it almost entirely disappears for high-mass fractions of Ti and Cr. This behaviour is more pronounced in the spectra of the SN 2001eh series. In both series, high Ti and Cr abundances result in an additional absorption feature at 3050 Å, mostly caused by Ti II. Further to the UV the trend again reverses, leading to more flux for the models with higher Ti and Cr abundance. Blue of ∼2700 Å reductions of Ti and Cr have only a small effect. In the optical spectrum, Ti and Cr predominantly affect the blue wing of the deep absorption around 4300 Å.

To quantify the change in the models better, we integrate the flux in different bandpass filtres of the WFPC2 instrument[6] and the standard *U*-band filtre (Bessell 1990). Fig. 4 shows the logarithmic representation of the Fe-model series of the SN 2001ep based models in Fig. 3 (upper right-hand panel) together with the shape and position of the different bandpass filtres in the upper panel.

Fig. 5 shows the integrated flux of the model spectra as a function of the change in the abundance of the respective set of elements

[6] See http://www.stsci.edu/hst/wfpc2.

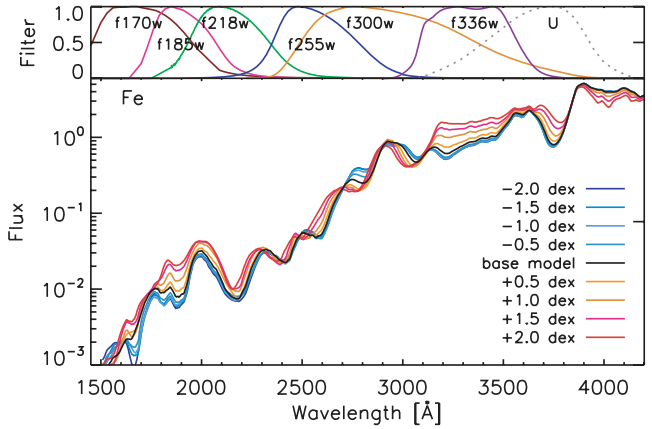

Figure 4. Logarithmic plot of the SN 2001ep model series with varying Fe content (cf. Fig. 3, upper right-hand panel). The upper panel shows the position and shape of the WFPC2 bandpass filtres used for the comparison of integrated flux shown in Fig. 5.

relative to the base model. The different lines and symbols correspond to the filtres indicated in the legend. Smaller values of Δm correspond to more flux in the corresponding filtre. Overall, the model series for the two base models show similar behaviour, although the absolute numbers are slightly different. The plots confirm what is visible in the spectra: the increase in Fe and Ti/Cr leads to a higher flux in some passbands, while the modification of ^{56}Ni has the opposite effect. The *U* band is almost unaffected by a decrease in heavy element abundances, while an increase always leads to more flux (although to a small degree in some cases). The feature that most strongly affects the *U* band is the re-emission peak bluewards of the Ca II H&K absorption. The largest variation is usually seen in the filtre centred around 1850 Å (*f185w*).

4.1.3 *Discussion*

The change in the UV flux with varying composition is mediated by two main effects. First, an increased content of heavy elements with a large number of lines in the UV increases the probability

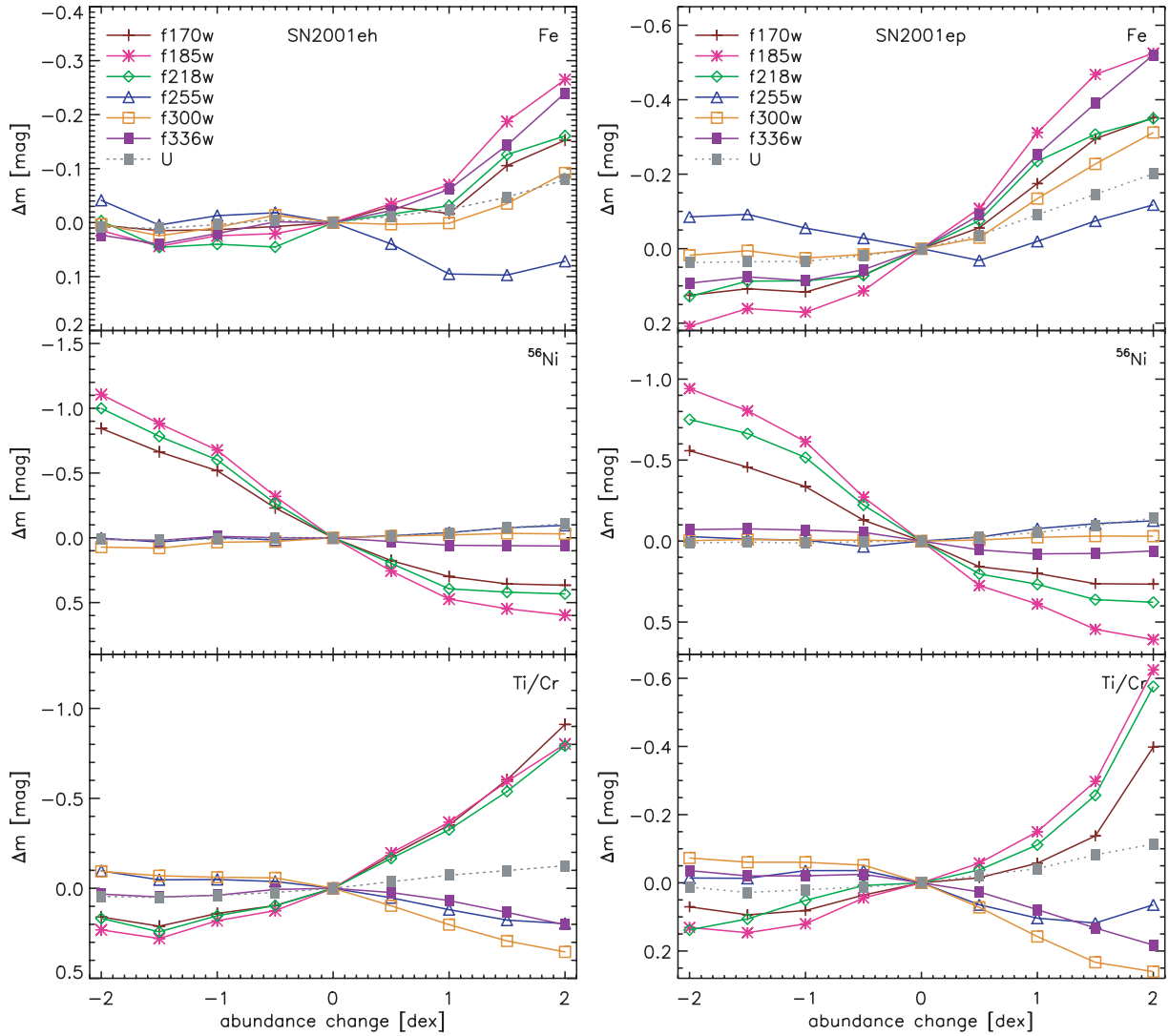

Figure 5. Comparison of the integrated flux in different bandpass filtres for the model series of SN 2001eh (left-hand panel) and SN 2001ep (right-hand panel). The curves show the change in magnitudes in a specific filtre band (cf. Fig. 4) relative to the base model versus the change in composition in the outer shell of the model.

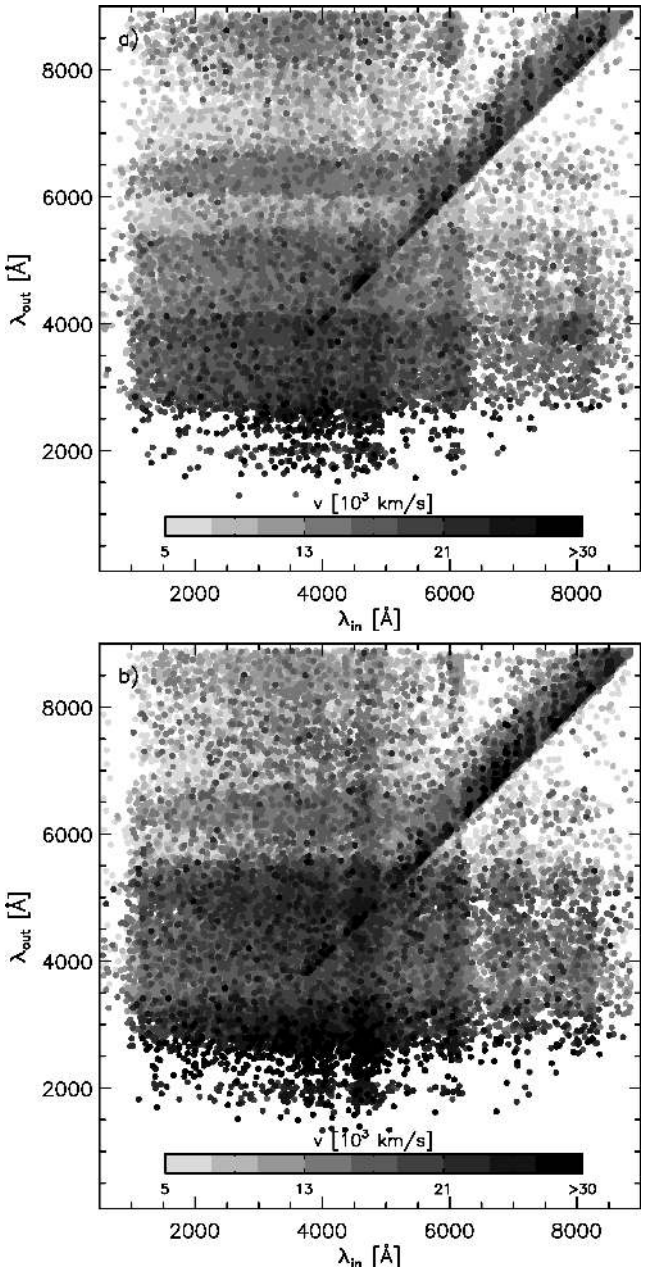

Figure 6. Final versus initial wavelength of all photon packets that emerge to infinity (cf. Mazzali 2000; Pinto & Eastman 2000). The grey shading indicates the velocity of the last scattering event. The darker a point is, the higher the velocity of the shell at which the photon packet encountered the last interaction with a line. (For wavelength pairs where more than one photon packet escapes, only the one with the highest velocity is shown. Note that a single point usually represents a larger number of photon packets.) The diagonal line represents all photons that are resonance scattered. All points above the diagonal are packets scattered to redder wavelengths, while all points below the diagonal represent packets that are scattered to bluer wavelengths through the reverse-fluorescence process. The upper plot shows the base model of SN 2001ep; the lower plot shows the same quantities, however, for the model, where the Fe abundance in the outer shell above 14 500 km s^{-1} was enhanced by 2 dex. The overall comparison shows that in the latter case, more photon interactions occur in the higher velocity shells (more darker points). It also shows that more packets are scattered from an initially red wavelength to blue and UV wavelengths (dark points with outgoing wavelengths $\lesssim$3500 Å below the diagonal).

for the reverse fluorescence to occur. Secondly, the increased line opacity leads to a stronger line-blocking effect, which affects the temperature structure and consequently the ionization structure in the ejecta.

The two plots in Fig. 6 illustrate the reverse-fluorescence effect in the Monte Carlo radiative transfer model for SN 2001ep. The points indicate the initial wavelength at which a photon package has been created versus the final wavelength at which it emerges from the envelope after the last scattering event. The grey-scale indicates the velocity of the shell where the last interaction occurred. Darker points correspond to higher velocities. Resonance scatterings that do not change the wavelength of the package are located on the diagonal.

The data in the upper panel are from the simulation of the base model for SN 2001ep; the data in the lower panel are from the model with high Fe abundance in the outer shells. Both simulations have a similar total number of emerging packets ($\sim$180 000), but the diagrams show only a fraction of this total number because many packets are located on identical positions in the wavelength grid. In the model with higher Fe abundance in the outer layers, the photons encounter more line events and are therefore more likely to be scattered out of their original wavelength. In the base model, 10 per cent of all packets emerging with $\lambda < 3750$ Å encounter their last interaction in a shell with $v > 20\,000$ km s^{-1}; in the model with high Fe abundance, this fraction is 20 per cent. Counting all packets emerging from the envelope regardless of wavelength, the fractions of packets encountering the last interaction at $v > 20\,000$ km s^{-1} are 3.9 per cent (base model) and 5.6 per cent (Fe enhanced).

The condition for the reverse-fluorescence process to lead to an increase in the UV flux is that the UV lines are saturated such that photons can escape from the lines without being re-absorbed immediately. Part of the UV enhancement seen in the models with increased Fe abundance is therefore caused by the presence of a larger number of saturated Fe lines in the UV. The decrease in UV flux in the models with enhanced ^{56}Ni abundance indicates that the dominating Co lines in those models are on average less saturated. Therefore, the optical depth in those lines increases with abundance.

The second consequence of the abundance variation in the outer shells is a change in the temperature and ionization structure caused by the change in line opacity. Fe-group elements have a large number of lines in the UV and blue part of the spectrum. The high velocities cause them to overlap and effectively prevent photons to emerge. The higher radiation energy density in the ejecta leads to higher temperatures and consequently a higher state of ionization.

Fig. 7 shows the mean radiation temperature (upper panel) and the ratio of doubly to singly ionized Fe (lower panel) for the SN 2001ep based model series in which ^{56}Ni is varied above 14 500 km s^{-1} (shaded area). A change to lower abundances does not have a strong effect but with increasing ^{56}Ni abundance a clear shift to higher temperatures and consequently doubly ionized species is induced. Backwarming extends the region affected to velocities lower than $v_{\rm shell}$ above which the actual variation has been imposed.

Pinto & Eastman (2000) discuss that in a gas having the physical conditions typically found in supernovae (low matter densities, high radiation energy densities) and dominated by sufficiently complex ions with a large number of possible line transitions, an equilibrium of the radiation field is established solely by radiative transitions. They regard this as an additional thermalization process that is not related to collisional and true continuum processes. In contrast to real thermalization, however, this equilibrium state does not couple the thermal properties of the gas to the radiation field. Therefore, the emitted spectrum depends only weakly on the temperature of

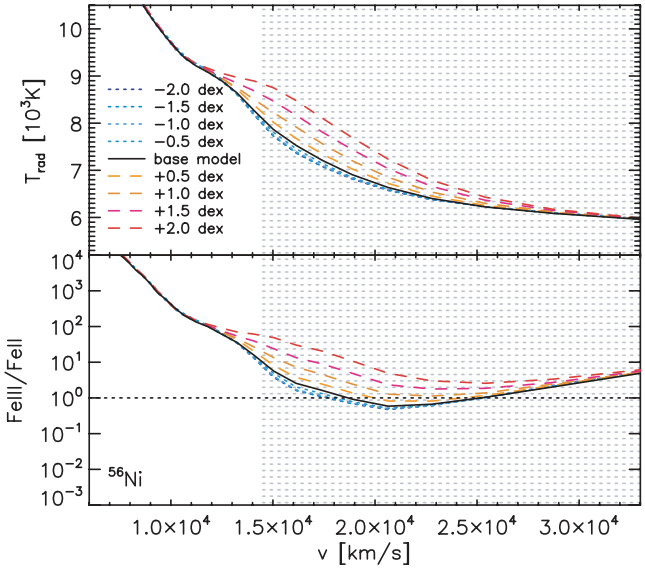

Figure 7. The upper panel shows the temperature as a function of velocity in the SN 2001ep model series where the abundance of ^{56}Ni was varied in the outer region above $v_{\rm shell} = 14\,500\,{\rm km\,s^{-1}}$ (shaded area). The lower panel shows the relative ionization of Fe III/Fe II for the same models. The models differ slightly even below $v_{\rm shell}$ because of the different number of photons scattered back into the envelope from outer layers depending on the heavy element abundance.

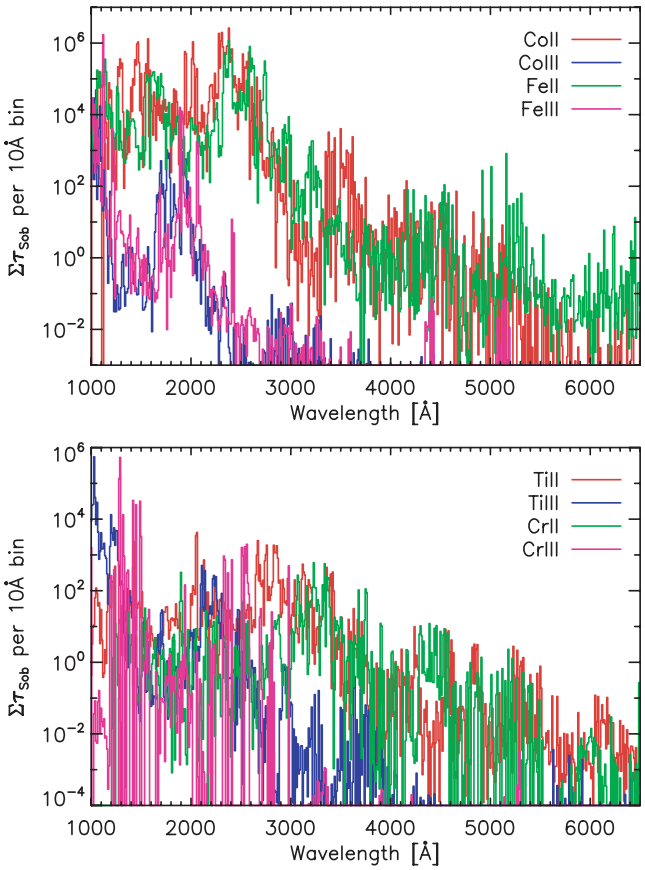

Figure 8. Sum of $\tau_{\rm Sob}$ for all the lines in a wavelength interval of 10 Å for the ions indicated in the plot legend. The Sobolev optical depths are derived for the model of SN 2001ep.

the gas (as long as the ionization does not change significantly with temperature). Instead, the spectrum reflects the distribution of line strengths as a function of wavelength. A change in the dominant species in the outer layers, either by a variation of the composition or the ionization state of the gas, can affect the density of spectral lines in the UV and may have a strong effect on the emergent spectrum. Fig. 8 shows the distribution of line strengths in terms of Sobolev optical depths for some of the relevant ions found in the mixture of SN Ia.[7] The qualitative difference of the distribution between different elements explains why different wavelength regions are affected when Ti and Cr are varied compared to the variation of Fe and Co. Overall the higher ionization stages tend to have fewer strong lines in the relevant spectral region. Therefore, a higher ionization decreases the total opacity. This introduces a feedback effect that prevents the opacity from growing arbitrarily with the abundance of Fe-group elements.

4.2 Variation of the density structure

4.2.1 Setup

For this series, we kept the inner structure of W7 out to a velocity $v_{\rm shell} = 15\,000\,{\rm km\,s^{-1}}$ and replaced the outer part with a power-law density $\rho \propto (v/v_{\rm shell})^{\beta}$ with power-law index β ranging from -5 to -16. The grey-shaded area in Fig. 9 shows the range of variation considered. For comparison, the density structures of the pure one-dimensional deflagration model W7 (Nomoto et al. 1984) and the delayed detonation explosion models DD4 (Woosley & Weaver 1994) and WDD2 (Iwamoto et al. 1999) are also plotted. The DDT models have somewhat more mass at high velocities (i.e. a shallower density gradient). The variation considered in the parametrized models covers the typical range of gradients for deflagration and delayed detonation models. All models are extrapolated to $v \sim 70\,000\,{\rm km\,s^{-1}}$ assuming power-law densities to ensure that the outer boundary does not affect the results.

Results the from multidimensional explosion models of Röpke et al. (2007) indicate that the 'bump' and the relatively sharp change in the gradient of the W7 deflagration model around $13\,700\,{\rm km\,s^{-1}}$ may be an artefact of the one-dimensional treatment. Multidimensional models tend to have a smoother density structure, although this can depend strongly on the assumptions made when averaging multidimensional models over angles to obtain a one-dimensional density structure. If the deflagration phase is followed by a delayed detonation, material is burned to higher velocities than in a pure deflagration because the flame is accelerated and can reach the outer regions of the white dwarf before the densities are too low for burning to proceed (Röpke & Niemeyer 2007).

At the epoch considered here, a modification of the density gradient at high velocities is expected to affect the UV part of the spectrum most strongly because the region where the optical spectrum is formed lies at much lower velocities. We restrict this study to one-dimensional explosion models because our radiative transfer models are spherically symmetric.

4.2.2 Results

Fig. 10 shows the model series for different gradients as well as the model based on the W7 density structure. The region which is

[7] The data shown in this plot are extracted from the SN 2001ep model but the distributions depend only weakly on the model.

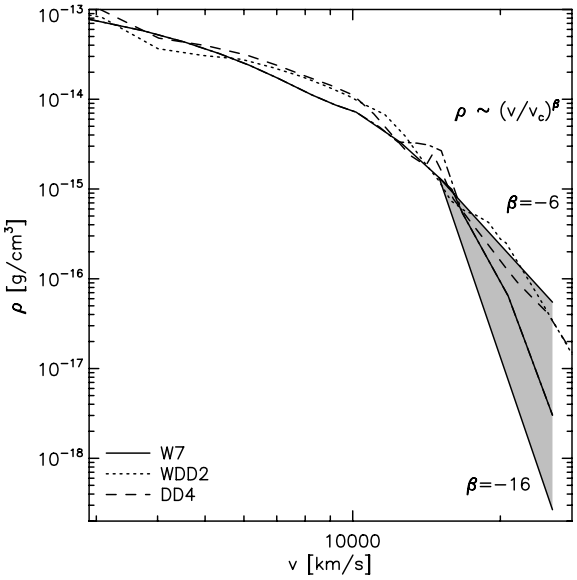

Figure 9. The model setup for the variation of the density structure in the outer part. The W7 density (solid line) is replaced by a power law with different power-law indices β between -5 and -16 (shaded area). For comparison, the two delayed-detonation models WDD2 (Iwamoto et al. 1999) and DD4 (Woosley & Weaver 1994) are also shown. For the spectral models, the density structures are extrapolated to higher velocities ($\sim$70 000 km s^{-1}) to avoid artefacts resulting from the outer boundary.

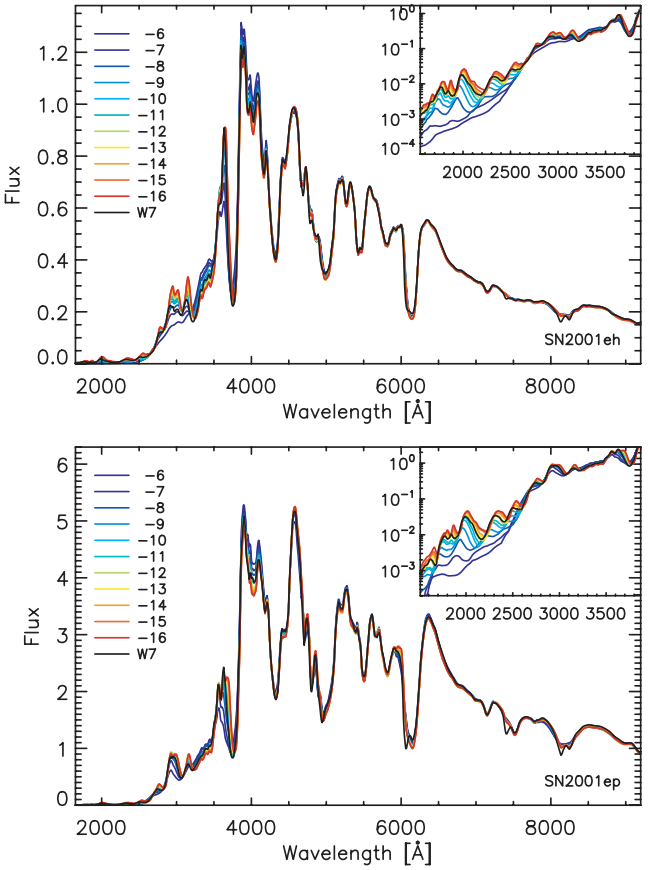

Figure 10. The full UV and optical spectra of the model series with varying power-law density above $v_{\rm shell} = 15\,000$ km s^{-1}. The upper panel shows the models based on the model for SN 2001eh and the lower panel shows those based on SN 2001ep. The colour coding refers to the power-law index β used for each model. For comparison, the black line refers to the original W7-based model spectrum, which is close to the $\beta = -12$ case in the outer part. The insert shows the UV part of the spectrum in logarithmic scaling.

mostly affected by the change is the UV bluewards of about 4200 Å. The rest of the spectrum remains largely unchanged.

The W7 model corresponds roughly to the model with $\beta = -12$. Models with a comparable or steeper gradient than the W7 structure show similar features that tend to become narrower for steeper gradients. In the models with shallower gradients, the features tend to become broader and shift bluewards for a power-law index of $\beta \lesssim -9$. In even shallower models, the structures become progressively less distinct and the flux in the UV below 2750 Å drops significantly. The overall effect is similar in both the model series except for the double-peaked emission feature centred around 3000 Å, which shows a stronger variation in the series of SN 2001eh.

Fig. 11 shows the integrated flux in the bandpass filtres shown in Fig. 4 for the model series with density variation (Fig. 10). The strongest variation is observed for the three bluest filtres (*f170w*, *f185w* and *f218w*), while other bands show only minor changes. For the very steep gradients, the flux is enhanced in those bands relative to the base model. As the gradient flattens, the flux drops by up to 2.4 mag in the *f185w* band. As expected, the results for the two supernovae are very similar. The difference at $\sim$3000 Å is not visible in the integrated flux because the *f300w* filtre is too broad.

We also computed models for the density structures of the two one-dimensional delayed detonation models WDD2 (Iwamoto et al. 1998) and DD4 (Woosley & Weaver 1994) using the same composition as in the base model for SN 2001eh. The resulting spectra are shown in Fig. 12. Both of the delayed detonation explosion models have a somewhat higher kinetic energy than W7 and thus more mass at higher velocities (cf. Fig. 9). The density gradients in the outer parts of both models are comparable and, therefore, the model spectra are not very different. Compared to the W7 model, the prominent features in the blue and UV are broader and shifted bluewards in the delayed detonation models. The same comparison for SN 2001ep shows qualitatively similar features but the difference to W7 is smaller.

4.2.3 *Discussion*

Line opacities scale with density. Therefore, the modification of the density gradient in the outer layers affects the wavelength range over which a photon can interact with a spectral line. Shallower density structures increase the effective range of Doppler-shifts from the line centre letting more lines overlap and leading to broader line features. This makes the line blocking at UV wavelengths even more efficient. Fig. 13 shows the temperatures and the ionization ratio Fe III/Fe II for the SN 2001ep model series with a varying density gradient. While the temperature varies only mildly for models with a density gradient steeper than W7, it becomes much higher in the outer parts for the models with very shallow density gradients. As in the models with varying composition, this behaviour reflects the increased heating of the ejecta by the higher radiation density caused by the more efficient line blocking. The ionization pattern shown in the lower panel of Fig. 13 roughly follows the temperature, with the exception that models with very steep gradients show a significant shift to higher ionization stages in the outer parts beyond $v \approx 17\,000$ km s^{-1}. Here, the low densities become the governing

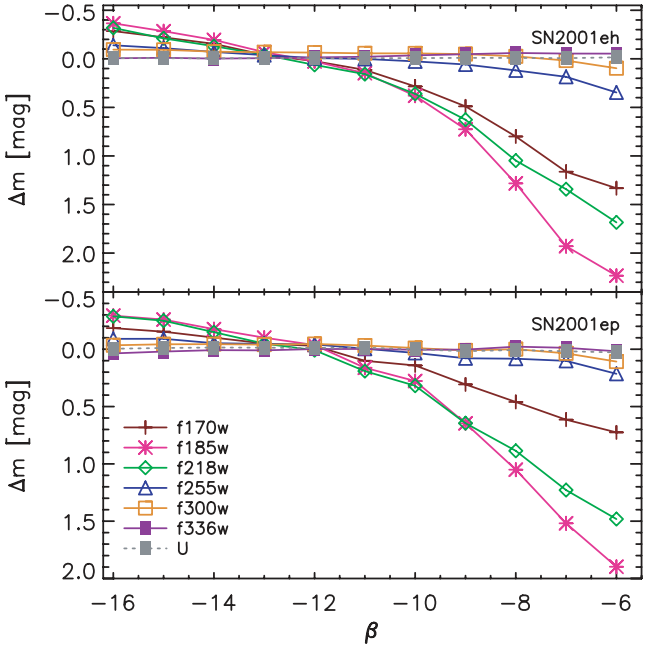

Figure 11. Variation of the integrated flux in the filtres shown in Fig. 10 relative to the original W7-based models.

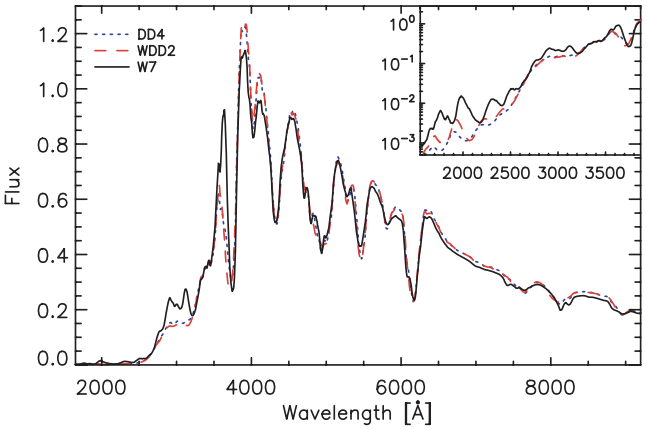

Figure 12. Spectra of the one-dimensional delayed detonation explosion models WDD2 and DD4 as well as the deflagration model W7 assuming an identical composition for all models. The series shown is based on the model for SN 2001eh.

factor that drives the ionization towards the doubly ionized species although the densities are too low to leave a significant imprint in the absorption features in the optical spectrum. The pattern is very similar for the other elements. The role of the distribution of line strength discussed in the previous section applies to this model series in the same way. The varying spectral appearance in the UV can therefore be qualitatively understood by the shift in ionization for the elements that provide the major source of opacity.

5 CONCLUSIONS

We analysed the spectra of two SNe Ia that have spectral coverage in the UV wavelength bands. Although the spectra were taken at very similar epochs, their appearances are different. The models show that the typical temperatures in the ejecta of SN 2001eh are

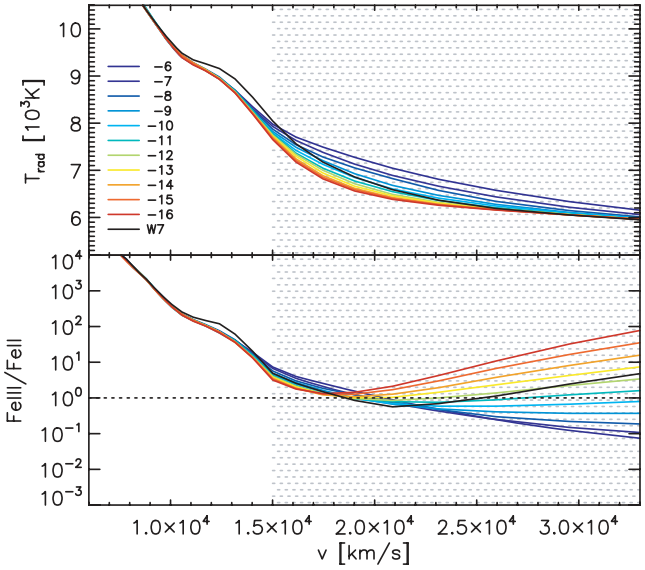

Figure 13. Similar plot as in Fig. 7 for the models with varying density gradients based on the model of SN 2001ep. The colour coding of the models is the same as in Fig. 10. The W7 model roughly corresponds to $\beta = -12$, however is somewhat shallower at lower velocities.

somewhat higher than in SN 2001ep. The shape of the spectrum of SN 2001eh is determined by absorptions of doubly ionized species (Fe III and Co III) while the shape of the spectrum of SN 2001ep is determined by lines of singly ionized iron-group elements (Fe II and Co II). The difference is especially visible in the UV bluewards of Ca II H&K. Based on these spectral models, we investigated the dependence of the UV flux on the metallicity and the density gradient in the outer layers of the ejecta. In one series of models, we varied the abundance of groups of heavy elements; in another series, we modified the density gradient in the outer layers and replaced the adopted explosion model with a power-law density structure that has different power-law indices.

The model series with varying composition shows that under certain conditions the UV flux may actually *increase* with increasing abundance of heavy elements while other models show the opposite behaviour. The physical process that dominates the formation of the UV flux in SNe Ia is a reverse-fluorescence process in which photons are absorbed at long wavelengths and re-emitted at a shorter wavelength in the blue or UV. Therefore, the shape of the spectrum is determined by the distribution of spectral lines as a function of wavelength. This distribution varies slightly for different elements, but is very sensitive to different ionization stages. A temperature change that results in a shift of the ionization balance directly affects the efficiency of line blocking in the UV, which couples back to the temperature. This feedback results in a non-linear response of the UV flux to changes in the metallicity. This wavelength region is therefore a valuable probe for the outer regions of explosion models, which do not leave a strong signature at longer wavelengths. To further study this effect quantitatively, a more realistic treatment of the temperature structure, consistent with the non-LTE state of the gas, should be used. In this work, we can only give a qualitative assessment of potential variations.

The density gradient mostly affects the breadth of observed line features. Shallow density gradients increase the velocity region over which a line can efficiently absorb and re-emit photons. For very shallow density structures, the densely clustered lines from

Fe-group elements in the UV cause individual absorption features to merge together resulting in a strong depletion of the flux. Steeper density gradients lead to narrower and more pronounced absorption and re-emission features.

Overall, the model series of both supernovae show the same qualitative changes. The main differences seen in the UV affect the shape and strength of the re-emission peak at ∼3500 Å, blue of Ca II H&K.

To conclude, a variation in composition and density of the high-velocity layers of the ejecta, which may be introduced by different progenitor environments or different degrees of mixing in the actual explosion, can have a significant impact on the observed UV flux even at later epochs when the optical spectrum is formed at much deeper layers. Depending on the exact physical conditions, a variation of metallicity can either reduce or increase the UV flux without leaving a strong imprint on the spectrum at longer wavelengths. For a better estimate of the magnitude and the scatter of the variation found in real supernovae, more UV observations of SNe Ia, preferably over a range of epochs, are needed. With the upcoming repair of STIS and the installation of the Cosmic Origins Spectrograph on *HST*, it should be possible to obtain additional UV spectra of SNe Ia that would be critical for such studies.

ACKNOWLEDGMENTS

We thank Stuart Sim for many helpful discussions and Stefan Taubenberger for his help sorting out the WFPC2 filtre functions. We also thank the anonymous referee for many constructive suggestions which helped to improve the manuscript. DNS acknowledges support from the European Union's Human Potential Programme *'Gamma-Ray Bursts: An Enigma and a Tool'*, under contract HPRN-CT-2002-00294 and the Transregional Collaborative Research Centre TRR33 *'The Dark Universe'* of the Deutsche Forschungsgemeinschaft. This research is supported by NASA/*HST* grants GO–9114 and GO–10182 from the Space Telescope Science Institute, which is operated by the Association of Universities for Research in Astronomy, Inc., under NASA contract NAS 5-26555. AVF is grateful for financial assistance from the National Science Foundation (NSF grant AST–0607485), the Sylvia and Jim Katzman Foundation and the TABASGO Foundation, without which the construction and continued operation of KAIT would have been impossible. Support for supernova research at Harvard University is provided, in part, by NSF grant AST–0606772. DNS, PAM, SB and RPK thank the Kavli Institute for Theoretical Physics, at the University of California, Santa Barbara, for its hospitality during the programme *'Accretion and Explosion: The Astrophysics of Degenerate Stars'*, supported in part by the NSF under grant PHY–0551164. This research has made use of the NASA/IPAC Extragalactic Data base (NED), which is operated by the Jet Propulsion Laboratory, California Institute of Technology, under contract with NASA.

REFERENCES

Abbott D. C., Lucy L. B., 1985, ApJ, 288, 679
Astier P. et al., 2006, A&A, 447, 31
Bessell M. S., 1990, PASP, 102, 1181
Blondin S., Tonry J. L., 2007, ApJ, 666, 1024
Blondin S. et al., 2006, AJ, 131, 1648
Bronder T. J. et al., 2008, A&A, 477, 717
Colgate S. A., McKee C., 1969, ApJ, 157, 623
Conley A. et al., 2006, AJ, 132, 1707
de Vaucouleurs G., de Vaucouleurs A., Corwin H. G., Jr, Buta R. J., Paturel G., Fouque P., 1991, Third Reference Catalogue of Bright Galaxies, Vol. 3. Springer, New York
Ellis R. S. et al., 2008, ApJ, 674, 51
Fabricant D., Cheimets P., Caldwell N., Geary J., 1998, PASP, 110, 79
Falco E. E. et al., 1999, PASP, 111, 438
Filippenko A. V., 1997, ARA&A, 35, 309
Filippenko A. V., 2004, in Freedman W. L., ed., Carnegie Observatories Astrophysics Series, Vol. 2, Measuring and Modelling the Universe. Cambridge Univ. Press, Cambridge, p. 270
Filippenko A. V., 2005, in Sion E. M., Vennes S., Shipman H. L., eds, Astrophysics and Space Science Library, Vol. 332, White Dwarfs: Cosmological and Galactic Probes. Springer, Dordrecht, p. 97
Filippenko A. V., Li W. D., Treffers R. R., Modjaz M., 2001, in Paczynski B., Chen W.-P., Lemme C., eds, ASP Conf. Ser. Vol. 246, Proc. IAU Coll. 183: Small Telescope Astronomy on Global Scales, Astron. Soc. Pac., San Francisco, p. 121
Fisher A., Branch D., Nugent P., Baron E., 1997, ApJ, 481, L89
Foley R. J. et al., 2008, ApJ, 684, 68
Foley R. J., Filippenko A. V., Jha S. W., 2008, ApJ, 686, 117
Ganeshalingam M., Li W. D., Chornock R., Filippenko A. V., 2001, IAU Circ, Vol. 7714, p. 4
Gehrels N. et al., 2004, ApJ, 611, 1005
Goldhaber G. et al., 2001, ApJ, 558, 359
Höflich P., Müller E., Khokhlov A., 1993, A&A, 268, 570
Höflich P., Khokhlov A. M., Wheeler J. C., 1995, ApJ, 444, 831
Höflich P., Wheeler J. C., Thielemann F. K., 1998, ApJ, 495, 617
Hurst G. M., Armstrong M., 2001, IAU Circ, Vol. 7712, p. 2
Hutchings D., Li W. D., 2001, IAU Circ, Vol. 7727, p. 1
Immler S. et al., 2006, ApJ, 648, L119
Iwamoto K. et al., 1998, Nat, 395, 672
Iwamoto K., Brachwitz F., Nomoto K., Kishimoto N., Umeda H., Hix W. R., Thielemann F.-K., 1999, ApJS, 125, 439
Jha S., Riess A. G., Kirshner R. P., 2007, ApJ, 659, 122
Junde H., 1999, Nucl. Data Sheets, 86, 315
Karp A. H., Lasher G., Chan K. L., Salpeter E. E., 1977, ApJ, 214, 161
Kasen D., 2006, ApJ, 649, 939
Kasen D., Thomas R. C., Nugent P., 2006, ApJ, 651, 366
Khokhlov A. M., 1991, A&A, 246, 383
Kirshner R. P. et al., 1993, ApJ, 415, 589
Krisciunas K., Hastings N. C., Loomis K., McMillan R., Rest A., Riess A. G., Stubbs C., 2000, ApJ, 539, 658
Leibundgut B., 2000, A&AR, 10, 179
Leibundgut B., 2001, ARA&A, 39, 67
Leibundgut B. et al., 1991, ApJ, 371, L23
Lentz E. J., Baron E., Branch D., Hauschildt P. H., 2001, ApJ, 557, 266
Lucy L. B., 1999a, A&A, 344, 282
Lucy L. B., 1999b, A&A, 345, 211
Matheson T., Jha S., Challis P., Kirshner R., Huchra J., 2001, IAU Circ, Vol. 7731, p. 3
Mazzali P. A., 2000, A&A, 363, 705
Mazzali P. A., Lucy L. B., 1993, A&A, 279, 447
Mazzali P. A., Röpke F. K., Benetti S., Hillebrandt W., 2007, Sci, 315, 825
Mazzali P. A., Sauer D. N., Pastorello A., Benetti S., Hillebrandt W., 2008, MNRAS, 386, 1897
Nomoto K., Thielemann F.-K., Yokoi K., 1984, ApJ, 286, 644
Panagia N., 2003, in Weiler K., ed., Lecture Notes in Physics, Vol. 598, Supernovae and Gamma-Ray Bursters. Springer, Berlin, p. 113
Pastorello A. et al., 2007, MNRAS, 377, 1531
Pauldrach A. W. A., Duschinger M., Mazzali P. A., Puls J., Lennon M., Miller D. L., 1996, A&A, 312, 525
Perlmutter S. et al., 1999, ApJ, 517, 565
Phillips M. M., 1993, ApJ, 413, L105
Phillips M. M., Lira P., Suntzeff N. B., Schommer R. A., Hamuy M., Maza J., 1999, AJ, 118, 1766
Pinto P. A., Eastman R. G., 2000, ApJ, 530, 757
Riess A. G. et al., 1998, AJ, 116, 1009

Riess A. G. et al., 1999, AJ, 118, 2675
Riess A. G. et al., 2004, ApJ, 607, 665
Riess A. G. et al., 2005, ApJ, 627, 579
Riess A. G. et al., 2007, ApJ, 659, 98
Röpke F. K., 2007, ApJ, 668, 1103
Röpke F. K., Niemeyer J. C., 2007, A&A, 464, 683
Röpke F. K., Hillebrandt W., Schmidt W., Niemeyer J. C., Blinnikov S. I., Mazzali P. A., 2007, ApJ, 668, 1132
Sauer D. N., Hoffmann T. L., Pauldrach A. W. A., 2006, A&A, 459, 229
Schlegel D. J., Finkbeiner D. P., Davis M., 1998, ApJ, 500, 525
Stehle M., Mazzali P. A., Benetti S., Hillebrandt W., 2005, MNRAS, 360, 1231
Tonry J. L. et al., 2003, ApJ, 594, 1
Truran J. W., Arnett D., Cameron A. G. W., 1967, Can. J. Phys., 45, 2315
Wood-Vasey W. M. et al., 2007, ApJ, 666, 694
Woosley S. E., Weaver T. A., 1994, in Bludman S. A., Mochkovitch R., Zinn-Justin J., eds, Supernovae. Les Houches, Session LIV. Elsevier, Amsterdam, p. 63

This paper has been typeset from a TEX/LATEX file prepared by the author.